Aligning conductive particles using magnetic field for enhanced piezoresistivity of cementitious composites

Zhuang Tian, Shaoqi Li and Yancheng Li*

School of Civil and Environmental Engineering, University of Technology Sydney, Ultimo, NSW 2007, Australia

Email: yancheng.li@uts.edu.au

Abstract:

The electrical and mechanical properties of the cement-based composites with magneto-aligned nickel powder are investigated in this study. The microstructure of the conductive pattern is examined by scanning electron microscope (SEM) and X-ray computed tomography (CT) scanning. It demonstrates that with the intervention of magnetic field, the electrical resistivity drops significantly and percolation threshold of the composites reaches at a lower filler concentration. The problems of high filler usage, low flowability and strength exists in the composites with randomly dispersed nickel particles can be addressed using the proposed method. Additionally, investigation on the influence of magnetic field intensity and duration shows that by adjusting these key parameters, the piezoresistive performance of the cementitious composites can be lifted. Under the superior piezoresistivity, giant gauge factor of the cement sensors is achieved which demonstrates an ability of stress/strain monitoring with high sensitivity.

Keywords: cementitious composites; nickel; self-sensing; piezoresistivity; magnetic field; alignment.

1. Introduction

Over the past few decades, the scale of modern infrastructure has become increasingly large, such as dams, bridges and tunnels. In these structures, cement composite is the most widely employed material due to its durability, strength, and low cost. However, large-scale buildings continue to be designed for a long service life but this involves considerable fatigue load, gradual environmental corrosion, and sometimes they are destroyed by or at risk of natural disasters. Nondestructive health monitoring, as a strategy to examine the functionality of a structure during its service life, is of increasing importance.

The self-sensing concrete concept was firstly reported by America researchers [1]. It was found that electrically conducting concrete had the potential to function as a non-destructive flaw detection technique due to the piezoresistive effect. Since then, theoretical models and experimental tests have been refined to prove this concept [2, 3]. To achieve satisfactory piezoresistive performance, a wide range of conductive fillers have been investigated [4], including carbon fibre [5-9], carbon nanotubes [10-14], carbon black [15, 16], carbon nanofibre [17], steel fibre [9, 18-20], nickel powder [21-24], graphite and graphene [25-28], conductive rubber [29, 30], and nano-scale inorganic substances such as Fe_2O_3 [31], etc. Among the composites with carbon based filler materials, numerous research works regarding the influence on the sensing behaviour have been carried out, including the mixing and dispersing methods [55], percolation threshold [56] and piezoresistive performance under different age and loading conditions [57] and mechanical properties. The results show that the carbon fibre is proved to be the most promising function material equipping the composites with better piezoresistive performance, easier dispersion and lower cost than carbon nanotubes, graphene nanoplatelets and carbon black.

Unlike most fillers used in the literature such as carbon-based materials, cement-based composites using nickel powder as conductive fillers have good self-sensing properties that can effectively act as sensors to monitor the health of structures. Nickel as a transition metal

material, is durable, malleable and ductile, and has relatively high electrical and thermal conductivities. Nickel nanoparticles have a high compressive strength of 34 GPa [32] and this generates the advantages of high permeability, conductivity, corrosion resistance. Consequently, nickel has been widely used in consumer and industrial products, for instance, stainless steel, coinage, rechargeable batteries, permanent magnets and plating on metal surfaces [33]. An adequate fraction of nickel powder can increase the flexural strength of cement binders by up to 48.1% [34].To date, much research on the electrical and piezoresistive properties of nickel powder filler have been carried out and the results proved their advantages and potential for engineering applications [21, 23, 35, 36]. Self-sensing concrete with nickel powder filler is proposed for weight-in-motion and traffic detection experiments [24, 37]. Laboratory data and on-site results indicated the excellent sensing capability of nickel-based cementitious composite, and under different ambient temperatures, the weight of front and rear wheels were transferred to electrical signals and detected by the cement-based sensors in real time [24]. The different weight (a minivan and a middle-sized passenger car) cause the sensor's resistance to change by 4% and 3%, respectively. Compared to conventional circuit chip sensors, cement-based sensors are more easily integrated into the concrete matrix for advantageous compatibility including lower maintenance cost, higher durability, and larger sensing volume [24, 38, 39]. Most of the self-sensing composites have a gauge factor between 50 and 500 [40], which are much higher than a commercial strain gauge with a gauge factor of 2. Mechanical properties are enhanced by fibre with high elastic modulus as well. For instance, the strength of the compact tension of the composites with 6.0 vol.% carbon fibre triples [39]. The steel fibre improves tensile strength from 5.6 MPa to 10.8 MPa [18]. Another benefit of the cement-based sensor is design flexibility. It can be embedded in any part of the structure elements or as a main bearing member for both functions of self-sensing and strengthening [41, 42].

However, the sensitivity of the sensor has a positive correlation with nickel powder percentage and the increased filler content undesirably reduces the strength of the sensor. Although the

FCR can reach -3.6% and -75% under 12.5 MPa compressive stress at 20 vol.% and 24 vol.% nickel powder content, respectively, the percolation threshold is as high as 24 vol.% of the composites. This is equal to approximately 250% by weight of cement under the water-to-cement ratio of 0.5 [21-24], causing the compressive strength to drop to 40 MPa [36] and a significant reduction in workability. This problem creates a dilemma for the sensor in that high sensitivity and high strength cannot be retained at the same time. Moreover, the sensors developed in the past share one common characteristic which is the isotropic pattern of filler distribution. According to prior research and applications, the sensors are focused on the measurement of uniaxial compression or tension which does not make the random distribution of filler fully functional.

It can be expected that the aligned nickel powder makes it easier to form the electrical conduction path which leads to the anisotropic electrical and piezoresistive properties of the cement-based sensors. Such cement-based composites can not only improve the electrical and piezoresistive sensing properties to a great extent, but also reduce the use of filler. Anisotropy properties have been demonstrated by the aligned steel fibre reinforced cement mortar and aligned nickel powder cement paste in other studies [43, 44]. This motivates the author to fabricate the aligned nickel powder cement-based materials and investigate its mechanical and physical properties.

In this research, by innovatively applying the magnetic field to ferromagnetic particles' redistribution, from random dispersed to a high-efficiency chain orientation, the piezoresistivity of the composites along the magnetic flux line can be drastically improved with reduced volumes required. For example, a high piezoresistivity could be achieved at 0.252 T magnetic field strength and a much lower particles concentration, which is only 5% in volume fraction of the composites without significant mechanical strength and modulus of elasticity dropping. The same effect could be obtained under 0.085 T magnetic field strength and 15% particle concentration. Moreover, smaller nickel particles have the advantages of being easy to disperse

into the solution, less chance of aggregation and cost-effective. The mechanism of this magnetic field intervention is that the conductive network including direct conduction and indirect electron hopping [2] is rearranged. Given the importance of the indirect tunnelling effect [45] that achieves piezoresistive performance, the magnetic field involvement mainly focuses on increasing the participation rate of particles in the network and optimising the micro-structure of ferromagnetic particles. Hopefully, this study may provide good data on conductive fillers redistribution in cement-based self-sensing composites system, and lead to a novel and cost-effective way that promotes the anisotropic piezoresistive performance of cementitious sensors.

2. Experimental

2.1 Raw material and sample fabrication

The matrix material of self-sensing cement-based composite is general purpose cement. The conductive filler is spiky spherical-shaped nickel powder with the diameter ranging from 3 to 7 μm. This type of nickel powder has highest comprehensive quality among current commercialised nickel particles, such as good conductivity, enhanced field emission effect and lower cost, approved by previous study [58]. Another nickel powder with an average diameter of 25 μm is introduced for computed tomography scanning purpose. The nickel powder specification is presented in Table 1. Superplasticiser (compound of 1~10% non-ionic surfactant (Amides, coco, N, N-bis) and <1% anionic surfactant (benzene sulfonic acid, dodecyl-, sodium salt)) is used to disperse the nickel powder in the water and promote the cement paste's workability. Anti-foam solution (silicon emulsion with <5% phosphates) is adopted to eliminate the air entraining effect caused by the superplasticiser when mixing.

Table 1. Specification of nickel powder.

Nickel powder Model	Diameter	Purity	Specific surface area (m^2/g)	Bulk density (g/cm^3)	Density (g/cm^3)	Electrical resistivity (Ω cm)	Shape	Colour
T123	3 - 7 μm	99.80%	0.4	1.8~2.7	8.9	6.8×10^{-4}	Spiky spherical	Dark grey
U25	8 - 35 μm	99.50%	0.025	3.2~5.5	8.9	6.8×10^{-4}	Spherical	Grey

It is essential to achieve appropriate flowability and viscosity for cementitious material. The workability is measured and compared using a flow table test following ASTM C230/C230M-21. Under a 0.4 water-to-cement ratio and the same superplasticiser percentage, with the increase of nickel particle concentration from 2.5% to 15%, the flow diameter drops from 210 mm to 150 mm. When it reaches 20%, the mixture completely loses flowability and leads to a failure of mixing and casting. As a consequence, high particle concentration and the morphology of nickel powder with spiky spherical shape could both result in non-homogeneity composites and a significant drop of flowability. To guarantee a similar rheological property for the samples with different particle concentrations, different water-to-cement ratio and superplasticiser proportion are adopted, as shown in Table 2. The composites flow diameters are controlled from 200 mm to 170 mm of the samples with 2.5%~15% particle content.

Table 2. Mixing design of cement-based nickel powder composites.

Nickel powder concentration (vol.%)	Water	Cement	Nickel powder	Superplasticiser (wt.%)	Anti-foam agent (vol.%)
2.5	0.4	1	0.16	0	0
5.0	0.4	1	0.34	0	0
7.5	0.4	1	0.50	1.0	0.1
10.0	0.4	1	0.72	1.5	0.15
12.5	0.45	1	0.92	2.0	0.20
15.0	0.5	1	1.13	2.5	0.25

Note: wt.% means the mass fraction of superplasticiser to cement; vol.% means the volume fraction of nickel powder or anti-foam agent to the composites. Water and nickel powder usage is based on the unit weight of cement.

The mixing process begins with solution preparation. Superplasticiser and defoamer are added to the water and the mixture is stirred for 5 minutes. Then nickel powder is added into the solution for a 10-minute mechanical mixing and 30-minute sonication process in an ultrasonic cleaning machine with a frequency of 40 KHz. Next, cement is added to the solution and mixed with a Hobart mixer for 5 minutes. After the mixing is finished, the paste is then poured into customised moulds with a dimension of 2.5 cm and 5.0 cm cubes, respectively. Two copper meshes with a size of 1.5 cm × 2.5 cm (aperture 0.71 mm, wire diameter 0.35 mm) are vertically placed with the distance of 1.5 cm into the 2.5 cm cube size paste samples as electrodes. The samples with a 5.0 cm cube size are for compressive strength testing.

To fabricate samples with chain patterned filler, the composites are taken to an electromagnet immediately after being cast into moulds. The electromagnet is powered by a DC power supply (PSI 8080-60 T LCD 1500 W) with a maximum current of 60 A and voltage of 80 V. Driven by the magnetic field, the ferromagnetic particles are constantly agitated and will move to a position where sufficient magnetic attraction can be provided to rearrange the particles into chain structures. Then the chain structures are fixed within the matrix due to the hydration process (Fig. 1). The electromagnet could generate maximum of 2.0 T magnetic field between two 60 mm pole faces and an air gap of 20 mm with 1% uniformity greater than 1 cm^3. A gauss metre serves to calibrate the magnetic flux density during the application of the magnetic field. In this research, the magnetic field strength is set at 0.085 T, 0.167 T and 0.252 T. The magnetic field duration is 30 s, 60 s and 90 s. For the samples with random dispersed particles, the magnetic factors are defined as zero. The sample categories are listed in Table 3. Each type of sample is duplicated into three specimens. After the designated durations of applying the magnetic field are reached, the samples are moved to a tray and cured in a chamber under a standard temperature of 18~22 ℃ and > 95% humidity for 28-day, then followed by a five-day oven drying at 50 ℃. The flow diagram of fabricating the proposed sensor is presented in Fig. 2.

Table 3. Samples with different nickel powder content and magnetic parameters.

Sample Name	Nickel powder concentration (vol.%)	MF intensity (T)	MF duration (s)
T-R02	2.5	0	0
T-A02	2.5	0.167	30
T-R05	5.0	0	0
T-A05-1	5.0	0.085	30
T-A05-2	5.0	0.167	30
T-A05-3	5.0	0.252	30
T-A05-4	5.0	0.167	60
T-A05-5	5.0	0.167	90
T-R07	7.5	0	0
T-A07	7.5	0.167	30
T-R10	10.0	0	0
T-A10-1	10.0	0.085	30
T-A10-2	10.0	0.167	30
T-A10-3	10.0	0.252	30
T-A10-4	10.0	0.167	60
T-A10-5	10.0	0.167	90
T-R12	12.5	0	0
T-A12	12.5	0.167	30
T-R15	15.0	0	0
T-A15-1	15.0	0.085	30
T-A15-2	15.0	0.167	30
T-A15-3	15.0	0.252	30
T-A15-4	15.0	0.167	60
T-A15-5	15.0	0.167	90

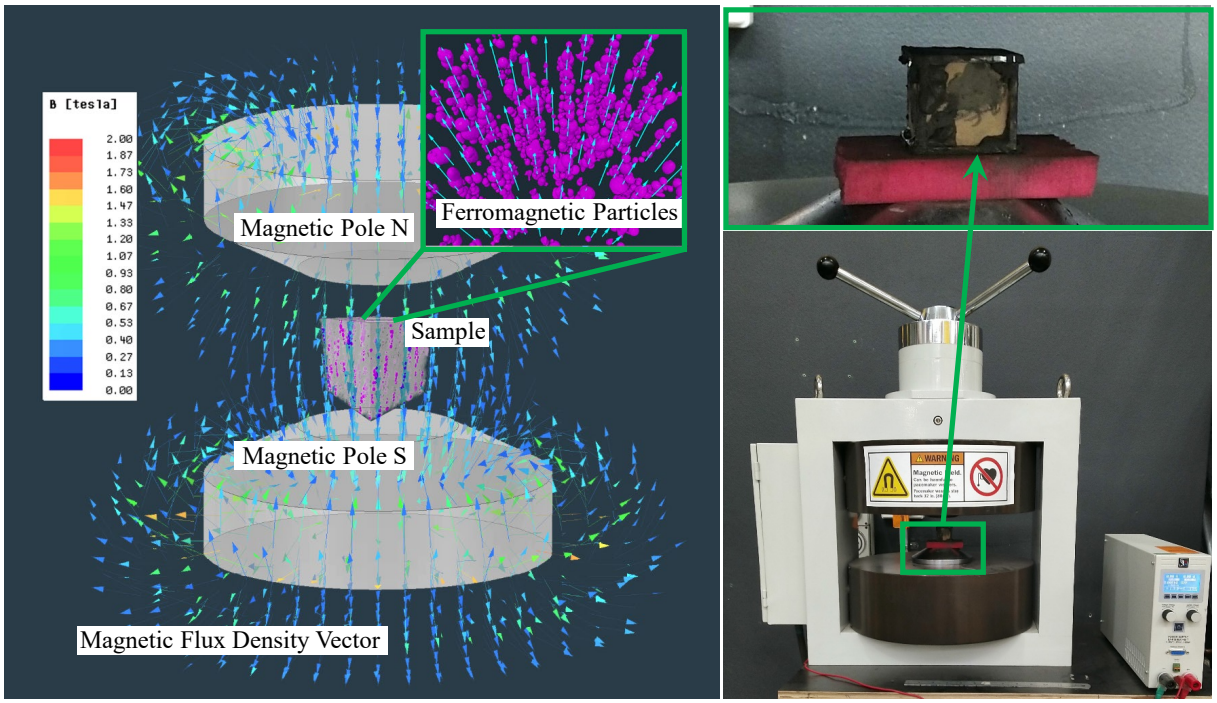

Fig. 1. Schematic illustration and experiment set-up of ferromagnetic particles alignment under the magnetic field.

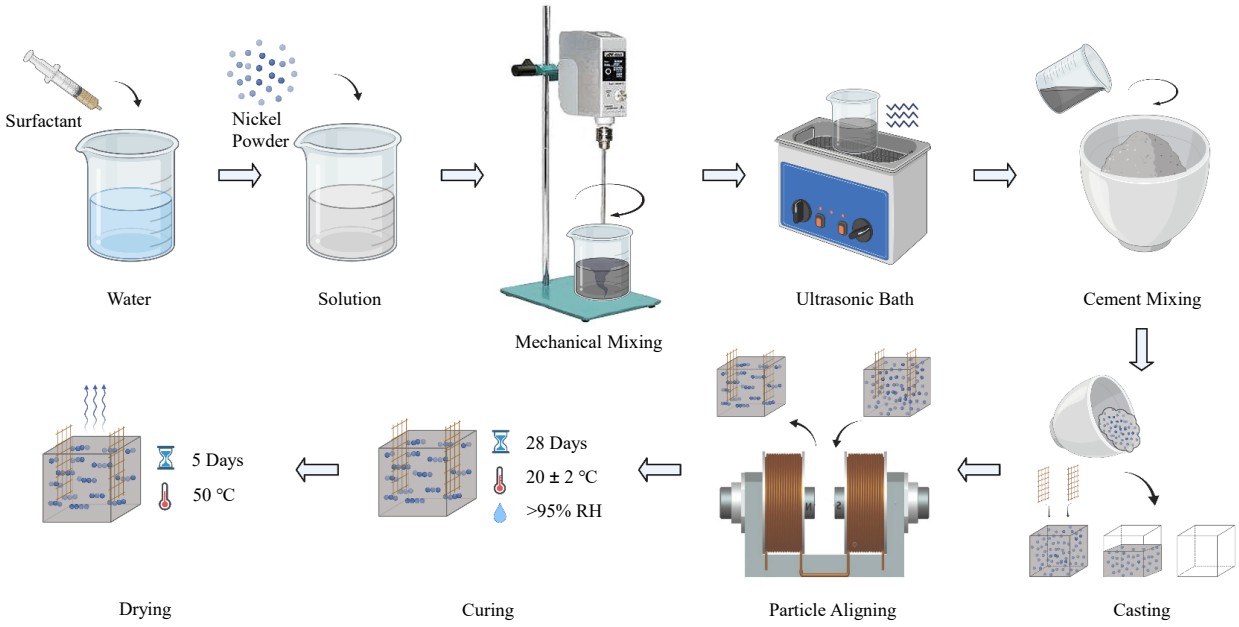

Fig. 2. Flow chart of fabrication of cement-based nickel powder self-sensing concrete.

2.2 Electrical properties measurement and morphology observation

As shown in Fig. 3, the electrical resistance is recorded by a multimeter (SDM3055 5½ Digit Dual-Display Digital Multimeter). All the measurements are carried out while the polarisation effect is stable which depends on the filler concentration and water content (lower filler concentration and higher water content result in a longer-lasting polarisation effect). In this study, the polarisation time takes 550 s, 290 s and 195 s for the samples with 5%, 10% and 15% nickel particles, respectively.

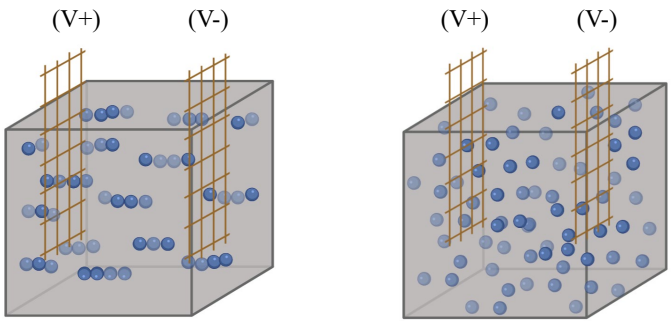

Fig. 3. Schematic diagrams for the measurement of electrical properties.

The piezoresistive test set-up is depicted in Fig. 4. Cyclic compressive loading is applied by a universal testing machine. The change in electrical resistance is recorded by the multimeter synchronously while loading. Mechanical properties are tested by another universal testing machine with a range of 500 KN.

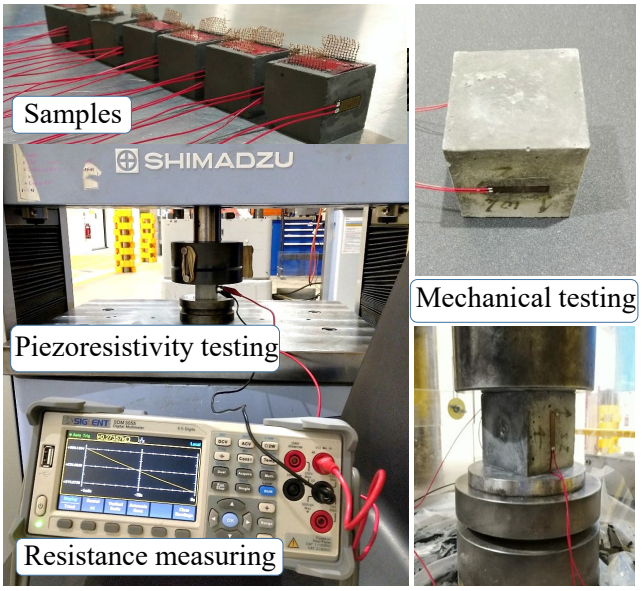

Fig. 4. Set-up of piezoresistive properties measurement and mechanical testing.

Regarding microstructure investigation, the particle morphology and distribution are inspected by a scanning electron microscope under an accelerating voltage of 15 KV. A 3D network formed by conductive particles is examined with a micro-CT scanner in a maximum resolution of 1 μm. Sample scanning data collected from the micro-CT is processed with 3D visualisation and analysis software.

3. Results and discussion

3.1 Morphology and orientation factor

3.1.1 CT observation

The aim of the chain structure is to provide unidirectional conductive paths that are consistent with the direction of external force. Then the conductive fillers are expected to work in a fully effective way. X-ray CT scanning is introduced for 3D observation of the spatial distribution of the chain structure. The scanning results can provide geometry data of the microstructure of the samples and visualised images following post-processing. From the 3D tomogram results (Fig. 5), short chains formation can be found inside cement paste with a length ranging from 0.02 mm to 0.15 mm depending on particle size and intensity of magnetic field. The chains are formed instantly while the magnetic field is engaged. Although the shape is affected by the cement hydration product in the initial setting stage of cement, the chains can maintain the formation during these complicated physical and chemical changes.

Besides the matrix properties, the size of magnetic conductive particles is another factor affecting the chain structure. As shown in Fig. 5a, the nickel particles with an average diameter of 5 μm are aligned under the magnetic field and fixed in the cement paste using the hydration process. The chains are coloured into groups according to the dimension to show the structure spreading out along the direction of the magnetic field. Limited by the resolution of the CT

scanning equipment (1 μm), the interparticle distance under this length could not be exhibited, thereby clearly resulting in an irregular rod shape rather than beads string shape. To show the chain in more detail, another type of composite with nickel powder with an average diameter of 25 μm is investigated. As shown in Fig. 5c, when the average particle diameter increases 5-fold, the micro expansion effect caused by the hydration process is relatively weakened. The chains are aligned with a better formation than those formed by smaller particles and the spherical shape is exhibited more clearly under the same scanning resolution.

Additionally, a simplified node and tube model in CT scanning post-process provides a more intuitive particle distribution in the composite, as shown in Fig. 5b. Most of the tubes that stand for short chains are along the direction of the magnetic field and have less connection with each other in transversal direction in 3D space. The average length-to-breadth ratio is 1.67 and the largest value is 6.25. The breadth includes not only the diameter of the nickel particles when the chain comprised single particulates, but also the width of several chains when they cluster together. Although the chains formed in the cement matrix are short, they have advantages in terms of electrical properties, e.g., piezoresistive effect. Unlike the long chains and closer particle distance which may lead to more electrical conductivity and indicate no piezoresistive behaviour, the discontinuity and curly shape of the particles in each chain and the gaps between chains provide space for conductive path deformation under loading. In this way the electron tunnelling effect is enhanced [46] and subsequently the self-sensing ability. For example, the sample has the tendency to contact under external compressive loading and return to the original position after unloading within an elastic range. Moreover, chains are independent of each other. This insulation prevents the conductive paths in the transvers direction of the chains, resulting in an anisotropic network.

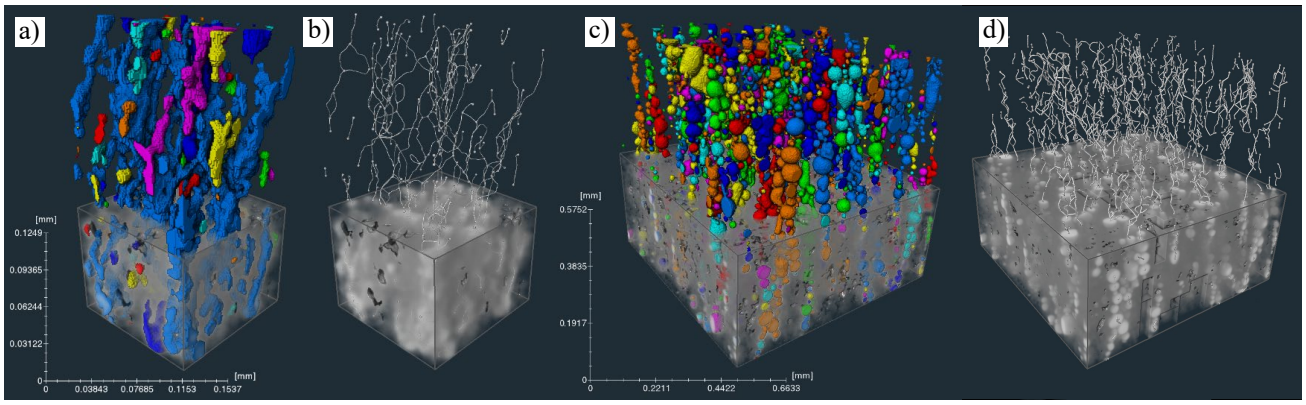

Fig. 5. X-ray tomography images of nickel powder: a) in average particle diameter of 5 μm, b) simplified node and tube model, c) in average particle diameter of 25 μm, d) simplified node and tube model. (Particle concentration is 5% volume fraction, 0.167 T magnetic field, sample size: a) -0.1 mm × 0.1 mm × 0.2 mm, c) -0.7 mm × 0.7 mm × 0.7 mm). To show the chains clearly in 3D, each chain is coloured separately according to its dimensions.

3.1.2 SEM observation

The SEM images clearly showed a slice of the patterned particles in the spatial samples. Higher resolution makes it possible to observe the interparticle distance and chains' length. It can be found that with the increase in magnetic field flux intensity, the length of chains is becoming longer (Fig. 6). For example, at 500 times magnification, the maximum chain dimensions in one microscope field of the composites with 10% particle content are 50.71 μm, 85.29 μm and 105.1 μm when the magnetic field strengths are 0.085 T, 0.167 T and 0.252 T, respectively. In the lower filler concentration composites with poor magnetic field strength (0.085 T and 0.167 T), chains appear short in length (20 - 30 μm, no longer chains are found), separate from each other, and evenly distribute in the composites. When the filler content increased to 15% the images under three magnetic field strengths present similar appearance. Short and long chains coexist in one microscope field. Despite long chains being bended or broke by the expansion of the cement hydration product, most of the patterns can still be recognised.

The appearances of the chains under different time durations are similar in various particle concentration groups. When the content rises from 5% to 15%, chains begin to join together. A longer period of magnetic field application has the same tendency as increasing the magnetic field intensity. For example, in Fig. 7i, a clear conductive path could be identified. Otherwise, due to the interference of scattered particles, it may not show greater visualising performance according to the SEM image. However, it can emerge as being more distinctive if placed under the X-ray scanning equipment and coloured into groups according to the dimensions of each chain, as shown in Fig. 5. From the SEM results, the morphology of the nickel particles aligned by various magnetic field strength and duration exhibits chain-structure in general. The pattern is more evident when the particles concentration is low, for example, 5 vol.%. With the increasing of particle concentration, the amount of chains gradually rise and form bundled-like structure. From the microscope aspect, the conductive network may behave more anisotropical under lower particle concentration.

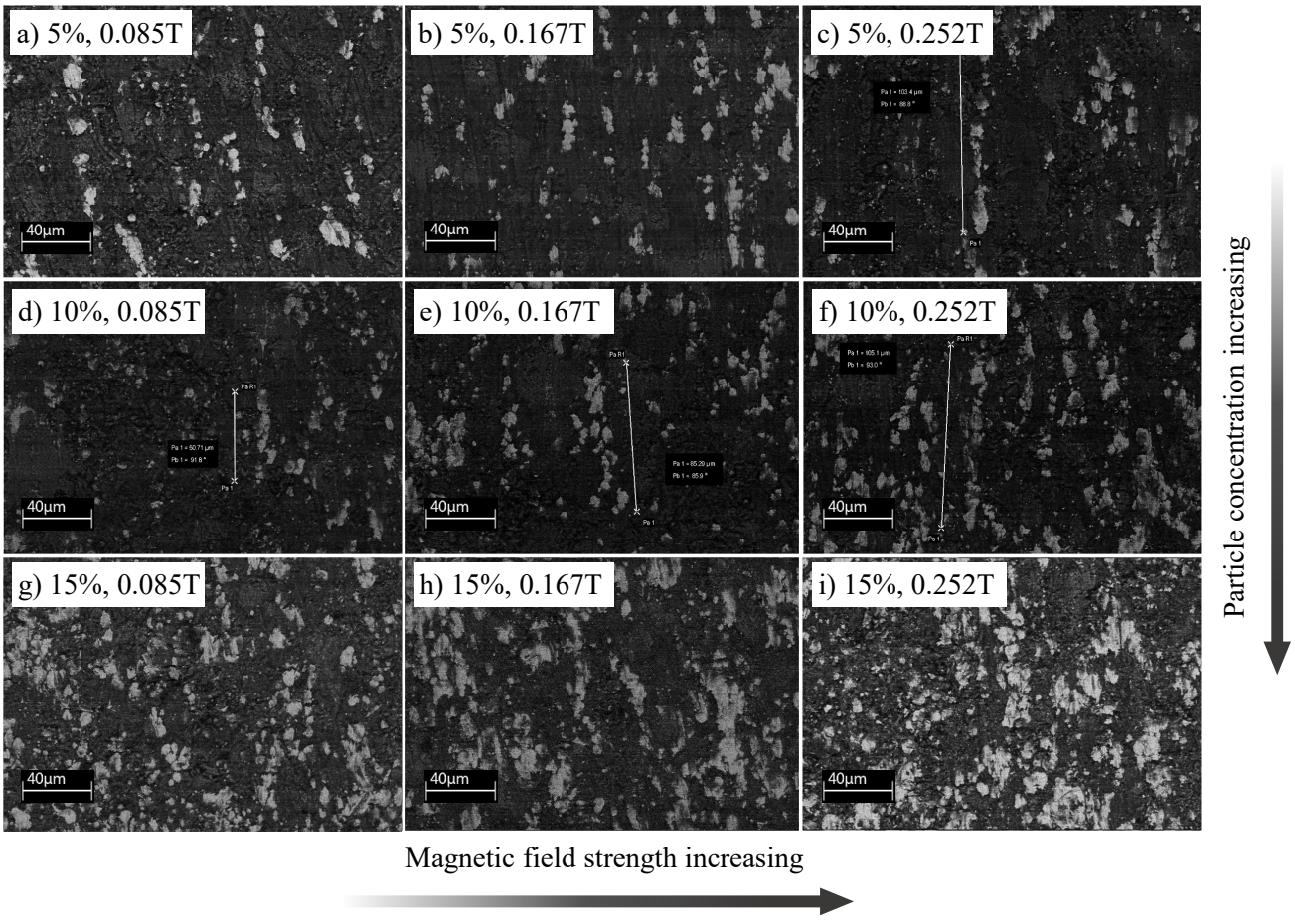

Fig. 6. SEM image of chain structure formed by different magnitudes of magnetic intensity (from 0.085 T to 0.252 T, 30 s duration) in 5%, 10% and 15% filler content.

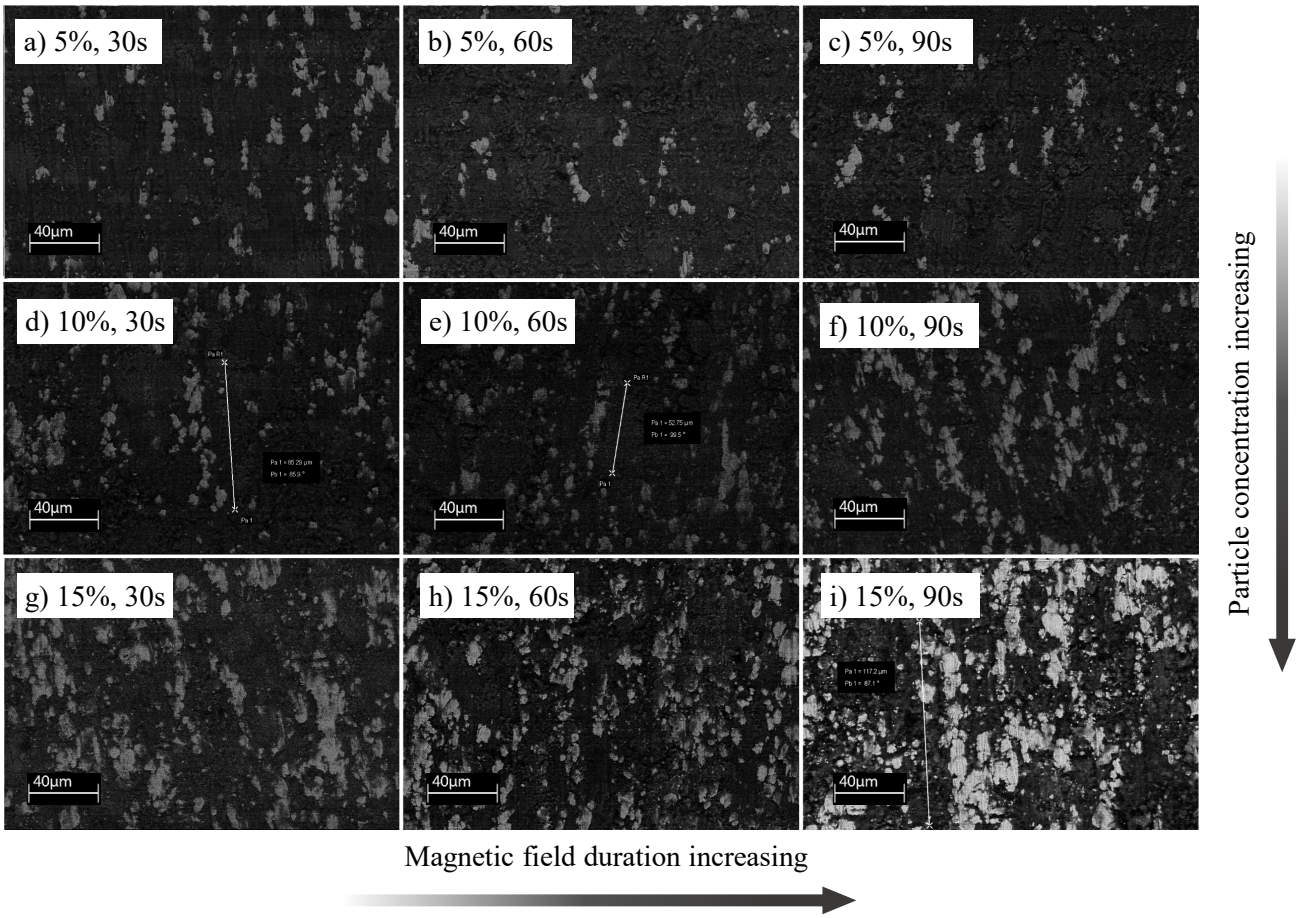

Fig. 7. SEM image of chain structure formed by different magnetic durations (from 30 s to 90 s, 0.167 T magnetic field flux intensity) in 5%, 10% and 15% filler content.

3.1.3 Orientation factor

Regarding the morphology of the chains, it is affected by the cement hydration process and displays an irregular shape and various lengths. In general, the average and maximal chain length increases with the rise of the magnetic field flux intensity and particle concentration, and slightly changes when the time duration increases. To evaluate the ferromagnetic particles participation rate of forming the chain structure, the chain efficiency factor is introduced which

is the ratio of the number of particles in chains to the number of total particles. As listed in Table 4, the factors are all above 0.90 indicating most of the particles take part in the chains formation effectively. The orientation of the chains is evaluated by the orientation factor which is expressed by Eq. (2). It can be seen from Table 4 that the factor ranges from 0.93 to 0.99, which means the chains are distributed efficiently along the direction of the magnetic field. Subsequently, this enhances the unidirectional conductive path under the proposed magnetic field strength and duration:

$$\eta_n = \frac{N_{pc}}{N} \tag{1}$$

$$\eta_\theta = \frac{\sum_1^{N_c} l\cos\theta}{N_c l} = \frac{1}{N_c}\sum_1^n \cos\theta_i \tag{2}$$

Where η_n is the chain efficiency factor, N_{pc} is the number of particles in chains, N is the total number of particles, η_θ is the orientation efficiency factor, N_c is the number of chains, and θ is the angle between the chains and direction of the magnetic field.

Table 4 The chain and orientation factors based on the SEM image analysis.

Particle concentration (vol.%)	Magnetic field strength/duration (T/s)	Number of scattered particles	Number of chains	Average chain lengths (μm)	Maximal chain lengths (μm)	Total number of particles	Chain efficiency factor	Chain orientation efficiency factor
5%	0.085 T	9	15	28.5	35.5	101	0.91	0.95
5%	0.167 T	9	17	29.6	47.3	93	0.90	0.99
5%	0.252 T	7	12	49	103.4	108	0.94	0.97
10%	0.085 T	15	8	53.3	75.6	249	0.94	0.98
10%	0.167 T	10	10	58.5	85.3	280	0.96	0.99
10%	0.252 T	8	12	62.6	105.1	260	0.97	0.98
15%	0.085 T	20	9	86.2	110.5	371	0.95	0.97
15%	0.167 T	16	8	99.2	145.3	346	0.95	0.93
15%	0.252 T	8	8	117.2	141.3	353	0.98	0.98
5%	30 s	9	17	29.6	47.3	93	0.90	0.99
5%	60 s	12	13	22.4	40.2	106	0.89	0.98
5%	90 s	10	15	24.9	36.5	115	0.91	0.97
10%	30 s	10	10	58.5	85.3	280	0.96	0.99
10%	60 s	8	32	58.2	80.7	304	0.97	0.97
10%	90 s	12	25	57.2	79.6	288	0.96	0.99
15%	30 s	16	8	99.2	145.3	346	0.95	0.93
15%	60 s	7	13	92	112.3	378	0.98	0.99
15%	90 s	7	9	90.5	115.8	410	0.98	0.98

3.2 Anisotropic electrical properties

The electrical properties of cement-based self-sensing composite are achieved through the network formed by conductive fillers. The resistivity continuously declines when the concentration of conductive particles increases. Fig. 8 illustrates the decreasing resistivity of the samples with two kinds of conductive networks formed by nickel powder, i.e., random dispersed and chain patterned. Under an identical concentration, the resistivity along the direction of magnetic field is much smaller than random distributed composites. Above 2.5% filler concentration, the resistivity drops rapidly. The values of samples with patterned fillers are 77.3%, 29.8%, 0.54%, 0.019%, 0.018% and 0.031% of those with random dispersed particles under 2.5%, 5.0%, 7.5%, 10%, 12.5% and 15.0%, respectively. The rapid drop from 5% to 10% content indicates the approach of the percolation threshold. Percolation threshold is a filler content under which all the conductive particles participate in the electrons transmission effectively, including electrons hopping effect and direct conduction. Most of the experiment design is based on the percolation threshold theory and arranging the particle concentration within this range.

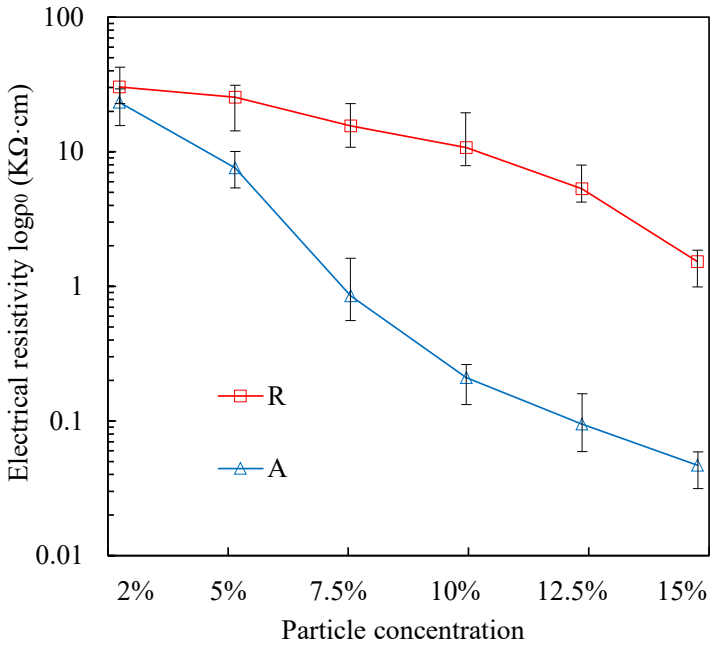

Fig. 8. Electrical resistivity of nickel powder (2.5% - 15% filler concentration) and cement-based composites with random and patterned conductive network (R-Random dispersed fillers, A-particles in chain pattern formed by 0.167 T and 30 s magnetic field).

From Fig. 8, it can be seen that in a random distributed filler system, there seemed to be no percolation threshold found, which suggests the filler concentration might not be high enough to reach the most effective conductive network. Only above 12.5% filler content does the resistivity begin to drop. In the literature, the percolation threshold of cement-based nickel powder composite is approximate 22% - 24%; it is a very high volume fraction and equals approximately 250% by weight of cement [36]. During the mixing process, when the filler proportion is beyond 15%, the cement paste could lose its workability significantly. However, when the ferromagnetic particles are aligned by the magnetic field, the electrical resistivity falls sharply between 5% and 10% particle concentration. This means the magnetic field intervention is able to: firstly, advance the percolation threshold along its direction; secondly, enhance the electrons transmission paths; and thirdly, make the network more effective with relatively less filler content.

In a random particle distributed composite, assuming the particles dispersed evenly in the matrix and ignoring the effect of voids and cracks, the composites consist of many cubes. The cubes and the particulates exist in the same quantity. Each cube includes a particle in the centre. Supposing the nickel particle is spherical in shape, then the cubic length can be calculated using the equation below:

$$L_c = D + D_{ps} = \sqrt[3]{\frac{\pi D^3}{6\varphi_B}} \tag{3}$$

Where L_c is the length of the cube, D is the particle diameter, D_{ps} is the distance between two particles, and φ_B is the particle volume fraction of the composite.

Then the critical volume fraction is expressed as written here:

$$\varphi_{Bp} = \frac{\pi D^3}{6(D + D_{ps})^3} \tag{4}$$

According to the quantum theory of the electron tunnelling effect, the value of D_{ps} is 10 nm. For the nickel particles that are spiky spherical-shaped, the effect is enhanced by the needle-points on the particle surface. Then D_{ps} increases several times, reaching above 1 μm. In this research, the average particle size is 5 μm, then in a random distributed composite, the very important volume fraction calculated according to Eq. (4) is 25%, is consistent with the majority of research on self-sensing cementitious materials using nickel powder. However, due to the high density of nickel, under this percolation threshold, the weight fraction of nickel powder to cement can be up to 250%, leading to a significant drop in mechanical strength and workability.

Under the intervention of the magnetic field, the particles are rearranged along the direction of the magnetic field. In other words, the distance between each particle is much smaller than the distance between each chain, resulting in an anisotropic conductive network. The 3D network formed by random particle distribution is altered to one dimension by the magnetic field, which

means the conductive paths in X and Y directions are reduced and transfer to Z direction. More specifically, only one third of the particles could be enough to form the conductive paths unidirectionally compared to an isotropic network. Additionally, with the increase in magnetic field flux intensity, the distance of interval particles (D_{ps}) decreased, resulting in the percolation threshold rising. However, with the further increasing of magnetic field strength or particles concentration, D_{ps} reduces significantly. Moreover, it further decreases as a result of compressive loading. Then the direct contact may dominate the conductive network, undermining the piezoresistive performance. The piezoresistivity from the change of D_{ps} is well reflected in the experiment result which is analysed in section 3.5.

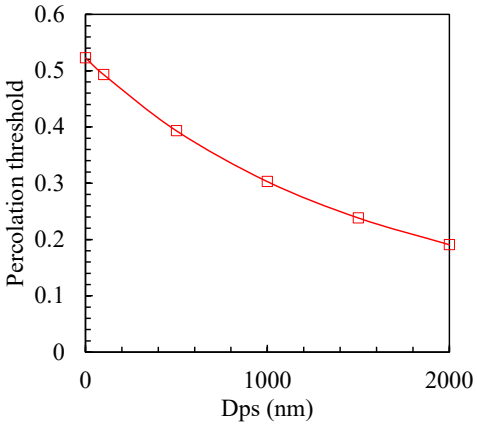

Fig. 9. The relationship between percolation threshold and particle distance (D_{ps}).

3.3 Anisotropic piezoresistive and mechanical properties

3.3.1 Anisotropic piezoresistive property of sensors under cyclic compressive loading

When cement-based self-sensing composites are subjected to external loading, the network formed by conductive particles is altered accordingly. Intuitive appearance is the change of resistance. For instance, the electrical resistance of cement-based sensors decreases with the increase of both compressive stress and the unloading of compression or loading of tensile

stress. The resistance change of the samples is presented below. Electrical resistance can be converted to resistivity which is calculated as electrical resistance per unit length and taking the sample size into account:

$$\frac{\Delta R}{R_0} = \frac{\Delta \rho}{\rho_0} + \frac{\Delta l}{l_0}(1 + 2\upsilon) \quad (5)$$

$$\rho_0 = R_0 \frac{A}{L} \quad (6)$$

Where Ro is the initial resistance, ρ_0 is initial electrical resistivity (Ωcm), $\Delta l/l$ is the strain, υ is the Poisson's ratio, L is the distance between the electrodes (cm), and A represents the cross-sectional area of the electrodes inside the composite (cm^2).

In cement-based sensors, the deformation or the strain of the sample is very small, compared to the sample's dimension, which means the change in resistivity is much larger than the strain. Eq. (5) is then written as shown below:

$$\frac{\Delta R}{R_0} = \frac{\Delta \rho}{\rho_0} \quad (7)$$

Thus, the piezoresistive effect could be represented by the fractional change of resistivity (FCR) [47]:

$$FCR = \frac{\Delta R}{R_0} = \frac{\Delta \rho}{\rho_0} = \frac{\rho_x - \rho_0}{\rho_0} \quad (8)$$

Where, ρ_x is the resistivity during loading.

In a random distributed filler system, the conductive network is formed isotopically. However, by redirecting the ferromagnetic particles into a proper order under the magnetic field, piezoresistivity is enhanced in the direction of the magnetic field exhibiting a unidirectional performance. Fig. 10 shows the FCR of 5 vol.% and 15 vol.% nickel powder and cement composites, respectively, under a 0.252 T magnetic field with compressive cyclic loading and unloading. The FCR matches the cyclic stress accordingly. The maximum FCR of 5 vol.% samples with patterned filler is -31.9%, 6.25 times larger than the samples with random fillers

which is -5.1%. With the increase in particle concentration to 15 vol.%, the FCR of the former decreases while the latter increases, reaching -25.8% and -16.1%, respectively. When the particles reformed from random distribution to the chain structure in the composites, the electron conductive path is altered as well, from 3D network to 2D chains along the direction of the magnetic field, or from the isotropic to the anisotropic network.

In the direction of the magnetic field, most of the electrons transmit unidirectionally along the chains. When the sample is subjected to compressive loading, shrinkage of the interface between particles in each chain occurs. Electron transmission that consists of direct conduction and electron hopping [2] becomes more effective and results in electrical resistance diminishing. Although the chains are not absolutely straight and isolated, there are sporadic particles and very short chains that connect the long chains forming conductive paths. It explains why the samples show lower electrical resistivity and better piezoresistive performance in this orientation. With the continuous increase in filler content, the network has the tendency to become saturated, and show poorer piezoresistive performance. As a consequence, with the intervention of the magnetic field, the percolation threshold can be reached in a lower filler concentration in the patterned network system.

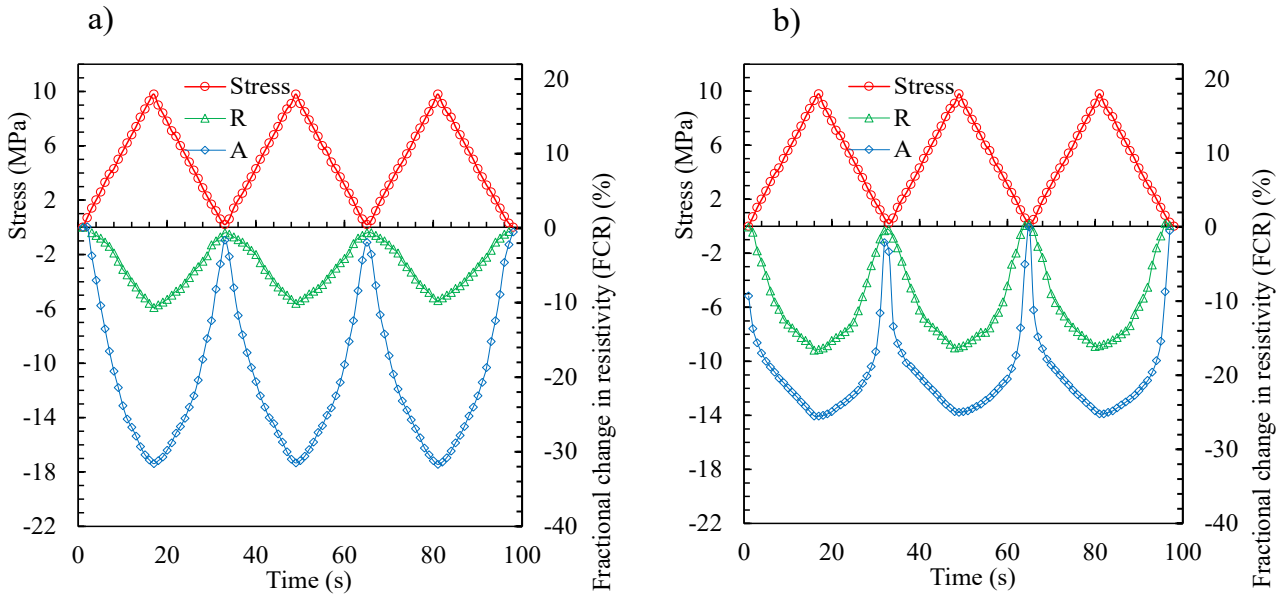

Fig. 10. Fractional change of resistivity of cement-based nickel powder composites in two different conductive networks (R-sample with random dispersed fillers, A-sample with chain pattern particles in the direction of compressive stress.) a). 5 vol.% filler content, 0.252 T magnetic field strength and 30 s duration. b). 15 vol.% filler content, 0.252 T magnetic field strength and 30 s duration).

In the direction of perpendicular to magnetic field, the piezoresistive performance decreases significantly. As shown in Fig. 11, the FCR under same conditions mentioned above drops to -1.6% and -3.9% with particle concentration of 5 vol.% and 15 vol.%, respectively. The values are only 1/3 to 1/4 of the composites with random distributed particles and 1/20 to 1/7 of the chian direction, showing anisotropic piezoresistivity. Especially under lower filler content, the anisotropic effect is significant. From a micro structure aspect, the increment of the distance between each chains result in less contact points of the conductive network in this direction. This experimental result is consistent with the micro structure analysis. Lower concentration is benefit to the strengthening of anisotropic network. In the meantime, the usage of filler material decreases and the cement mixing process becomes easier.

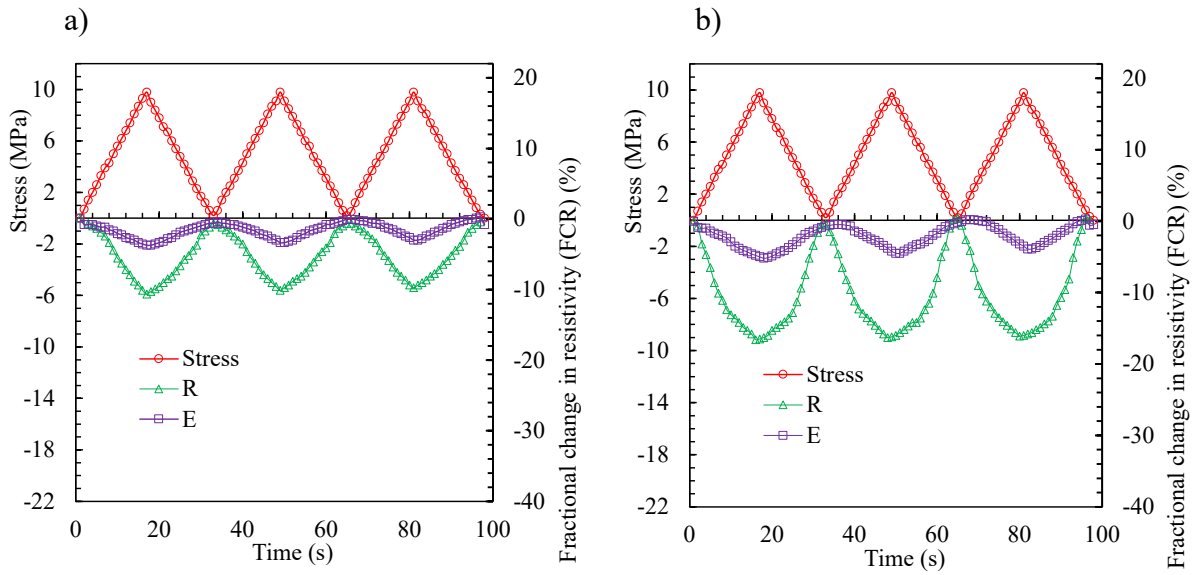

Fig. 11. Fractional change of resistivity of cement-based nickel powder composites in two different conductive networks (R-sample with random dispersed fillers, E-sample with chain

pattern particles in the direction perpendicular to the stress.) a). 5 vol.% filler content, 0.252 T magnetic field strength and 30 s duration. b). 15 vol.% filler content, 0.252 T magnetic field strength and 30 s duration).

3.3.2 Compressive strength

After 28 days curing under standard conditions, the 5.0 cm cubic samples are placed on a universal testing machine for mechanical strength test following ASTM C109/C109M-20b. Experiment results show that the compressive strength decreases when the nickel filler concentration increases (Fig. 12). The original 28-day ultimate strength of reference plain cement paste in this project is 62.3 MPa. When the nickel powder concentrations are 5% and 10%, the strengths of the samples are approximately 51.4 MPa and 47.0 MPa, which are 82.5% and 75.4% of the reference samples. However, it drops significantly to 37.5 MPa after reaching 15% particle content, only 60.2% of the reference samples. The main reason of the reduction of mechanical strength may be attributed to the air entraining effect caused by the water reducer especially an increasing usage under a high particle content. It may also result from the morphology of the nickel powder. Although the spiky shape is beneficial to electrical properties, these nano-scale thorns on the surface of the particle are relatively weak. Moreover, when particles make contact with each other, gaps may be formed among the thorns which cannot be filled with the cement hydration product. Under compression deformation, these voids and thorns can lead to the concentration of stress and strength deduction. However, as discussed in the previous section, the same piezoresistive performance can be achieved under a much lower nickel particle concentration. For example, 5 vol.%, rather than random filler system with 15 vol.% filler content, means that the compressive strength is guaranteed, or the sample has high sensing property and mechanical strength at the same time.

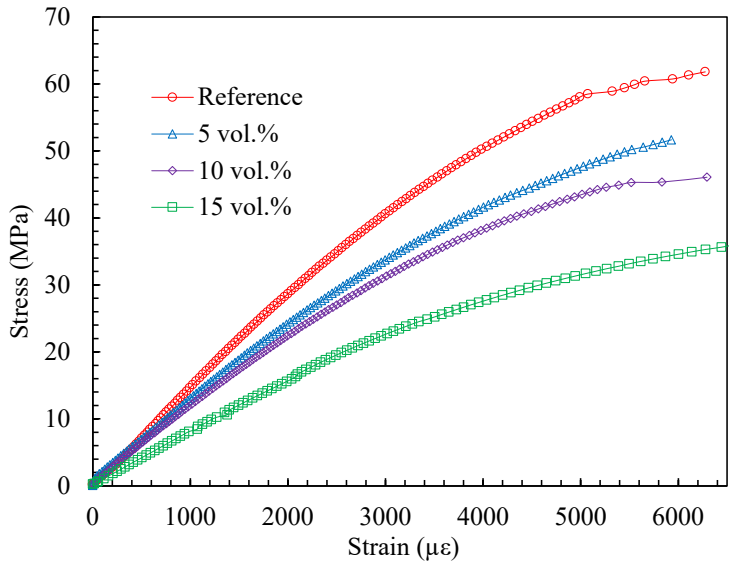

Fig. 12. Compressive strength of cement-based and nickel powder composites in 5%, 10% and 15% particle content (nickel particles are aligned by 0.252 T and 30 s magnetic field).

3.3.3 Modulus of elasticity

As shown in Fig. 13, the modulus of elasticity (MOE) of the samples has a similar trend with the compressive strength. The MOE of plain cement paste is 15.5 GPa. 15.0 GPa, 11.9 GPa and 10.1 GPa, which are the values for the samples with 5%, 10% and 15% random dispersed nickel particles. The numbers drop slightly to 15.6 GPa, 12.1 GPa and 9.6 GPa for the composites with patterned nickel powder, respectively. It is worth noting that the MOE of samples with 5% nickel powder does not drop significantly. In fact, the value of the specimen with patterned fillers is slightly higher than the reference one. Referring to high content, for instance 15%, the MOE samples with a chain filler structure is slightly lower than that with random filler. This may result from the increasing application of surfactant when dispersing high content particles into the solution before mixing. The negative air entraining effect inevitably reduces the strength and MOE. Similar to the properties of mechanical strength, high MOE value is

acquired under a low patterned filler concentration with an impressive piezoresistive performance.

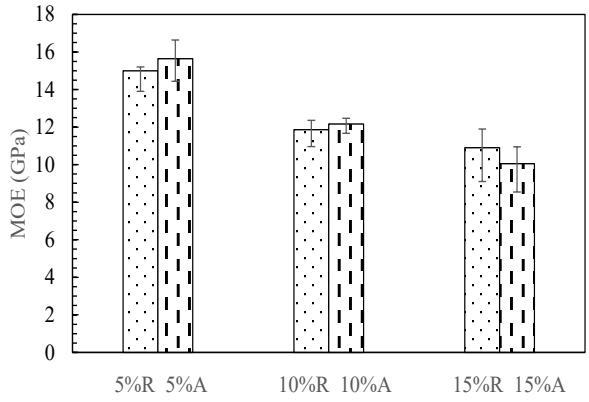

Fig. 13. The modulus of elasticity (MOE) of cement-based and nickel powder composites in 5%, 10% and 15% content and with random and patterned fillers. (R- nickel powder random distributed, A- nickel particles aligned to the direction of compression)

3.4 Sensitivity of the sensors (Gauge Factor)

Another factor to evaluate sensor sensing ability is gauge factor which is written below:

$$GF = \frac{\frac{\Delta\rho}{\rho}}{\frac{\Delta l}{l}} = \frac{FCR}{\varepsilon} \tag{7}$$

Gauge factor (GF) is the ratio of FCR to strain, which means high performance sensors can achieve great FCR values under small deformation when subject to external loading. In this research, one cycle of 12 MPa compressive stress is pre-loaded to: firstly, examine and eliminate tiny brittle fractures in the elastic range; and secondly, stabilise the contact resistance between electrodes and composites. Then, GF test is carried out in a low compressive stress (0 – 10 MPa) to guarantee a linear material deformation and reversible change of electrical resistance. The surface of the samples is sandpapered to ensure an even compressive stress loading. Two strain gauges are attached to the opposite sides of the cubic samples to achieve a balanced average value.

When the GF value is larger than 500, the sensors show a significant piezoresistive performance [40] and this is known as giant piezoresistivity. Among cement-based self-sensing composites, most of the GF value is between 50~500 (when the samples under tensile loading, the value is negative), in which the particulates distribution is random. In this research, the highest anisotropic GF value is 3626 (5% nickel powder concentration with a chain structure along 0.252 T magnetic field orientation) within a strain range from 0 – 80 με, the other two GFs in the same group are 2607 and 2941, despite the fluctuation, this group still shows distinct sensitivity. Regarding the groups under 0.167 T and 0.085 T magnetic field, respectively, the average GFs are 2140 and 1518 Fig. 14a indicates the GF of cement-based sensors under compressive loading available in the literature. It can be seen that the composite in this study has a quite high fractional change in resistivity within a small range of strain after the conductive filler aligned into the chain structure. As shown in Fig. 14b, the FCR on maximum GF curve shows a non-linear relationship with the strain. It appears to be caused by the strong magnetic field density. The distance between each particle in the chains is narrowed by the magnetic field flux, and it especially becomes closer under a high magnetic field intensity. With the increase in compressive loading, the electron could transmit directly, rather than engage in electron hopping or the tunnelling effect. Thus, the curve chart tends to be flat at the end of elastic deformation. Additionally, since the cement material is brittle, the deformation capacity is decreased when it enters into plastic range, even in high strain part of the elastic regime, presenting non-liner shape on the strain curve. Overall, the giant gauge factor confirms the great potential for fabricating anisotropic cementitious sensors with high unidirectional sensitivity and effectiveness.

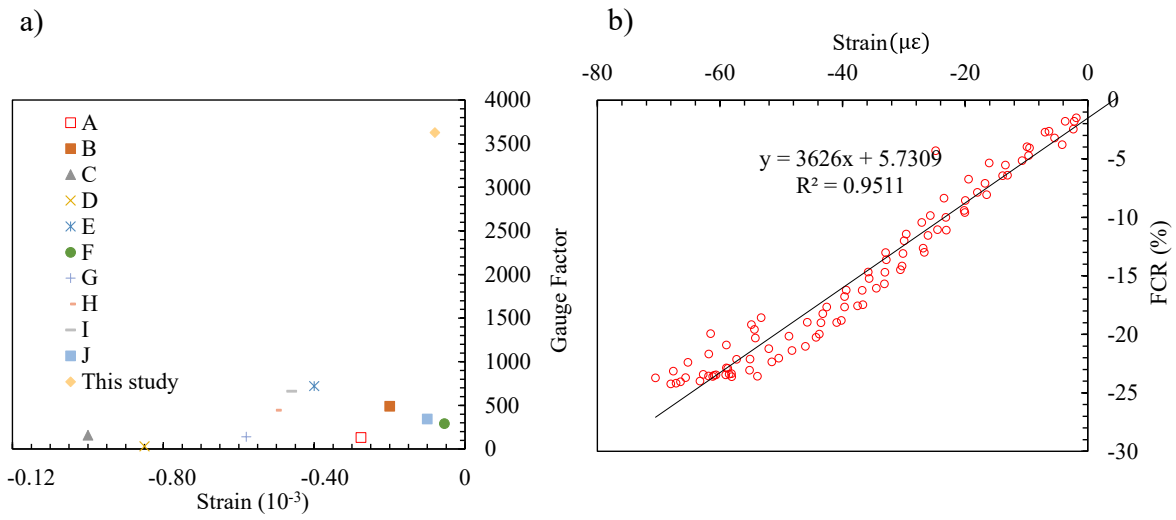

Fig. 14. Comparison of isotropic gauge factors in literature of cement-based self-sensing composites under compression and the maximum anisotropic GF in this study. (A: [48], B: [29], C: [49], D: [16], E: [7], F: [50], G: [51], H: [52], I: [53], J: [54])

3.5 Impact of magnetic field intensity and duration on self-sensing performance

Two key factors involved in the forming chain-like structure in cementitious composites are magnetic field intensity and duration. From Fig. 15a, the electrical resistivity decreases with an elevation in magnetic field strength and action time for cement-based nickel powder composites in the direction of the magnetic field. This field's duration wields less influence on resistivity compared to magnetic field strength (see Fig. 15b). Both factors are able to change the electrical resistivity more under a higher filler concentration (15%). The composites with spiky nickel powder have resistance variation over a large range, especially generating a significant drop when the magnetic field intensity rises to 0.252 T.

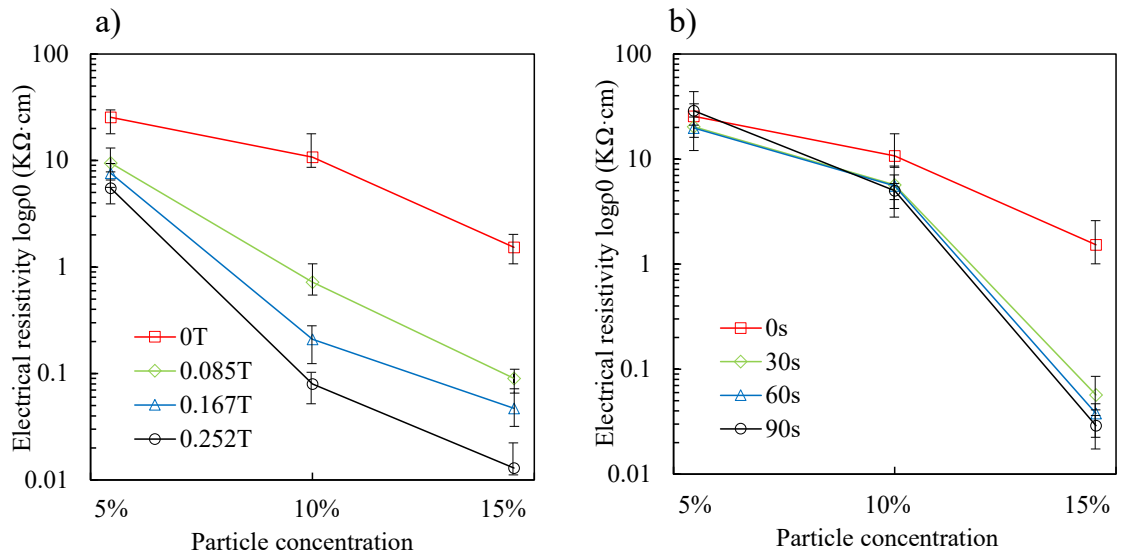

Fig. 15. Electrical resistivity of the samples under different a) magnetic field flux strength and b) duration.

Regarding the FCR of the specimens under different magnetic field parameters, as shown in Fig. 16, the peak value increases with rising magnetic field intensity in the 5% filler concentration, from -14.5% to -19.4%, and then -31.9%. When the nickel powder content increases to 10%, the FCR shows a similar trend to that of the 5% content. However, at 15% filler content, it has a similar FCR value under each magnetic field magnitude, approximately -30%, which means that in a higher filler concentration, a low magnetic field strength could promote the FCR significantly. It is worth noting that for the composites with 15% nickel particles, the FCR slightly drops, from to -33.9%, -31.2% to -25.0%, with magnetic field intensity increasing from 0.085 T, 0.167 T to 0.252 T, respectively. This reverse trend indicates that the network may become gradually saturated and the direct electron conduction will tend to dominate the conductive paths. The flat section on either side of the peak value on the 0.252 T curve of the samples with 10% and 15% particles verify this phenomenon as well. When the slope of the curve decreases, the piezoresistive performance falters, which seems inevitable. Since the elastic modulus of nickel (207 GPa) is much higher than of the cement paste, most of

the deformation of the composite is from the voids shrinkage, followed by the cement hydration product.

After the gaps and the voids are closed by compressive stress, the pace of deformation slows down. If the conductive network inside the composite is electrically saturated before the material's deformation, then the piezoresistive performance is weakened or ended beforehand. This is the pre-saturated state (Pre-SS). In contrast, when the sample deformation occurs within the conductive network saturation, there is residual piezoresistivity beyond the test strain. Then it is defined as post-saturated state (Post-SS). For example, in Fig. 16a, the piezoresistive performance is in the Post-SS under the 0.252 T magnetic field. Meanwhile the samples with 15% particle content are in the Pre-SS (Fig. 16c) stage under the same magnetic field. In a random filler dispersed composite, the network cannot be changed unless particle concentration is altered. However, with the intervention of magnetic field, the electrical property of cement-based composites indicate flexible ability. To be more specific, by adjusting the magnetic field strength in the fresh stage of the paste, the network formed by the nickel particles could vary significantly. Thus, the critical threshold of the Pre-SS and Post-SS can be found and the piezoresistivity is likely to be optimised. Additionally, it can be seen from Fig. 16 that the FCR of the samples with 5% conductive particulates and under 0.252 T magnetic field have the same value as those with 15% particles and under the 0.085 T magnetic field. In other words, same sensor piezoresistivity is achieved by increasing magnetic field strength with a smaller particle concentration. Although the results are similar under these two scenarios, the former has its advantages. Given that high magnetic field strength is relatively easy to achieve, low particle concentration means cost savings. Lower filler content is easier to disperse into the composites and has less chance of forming particle aggregation or clusters. Moreover, from the SEM images and FCR curve chart, samples with lower filler content exhibit a much more linear piezoresistive performance. More importantly, the compressive strength and MOE are much higher under lower particle content than a high concentration.

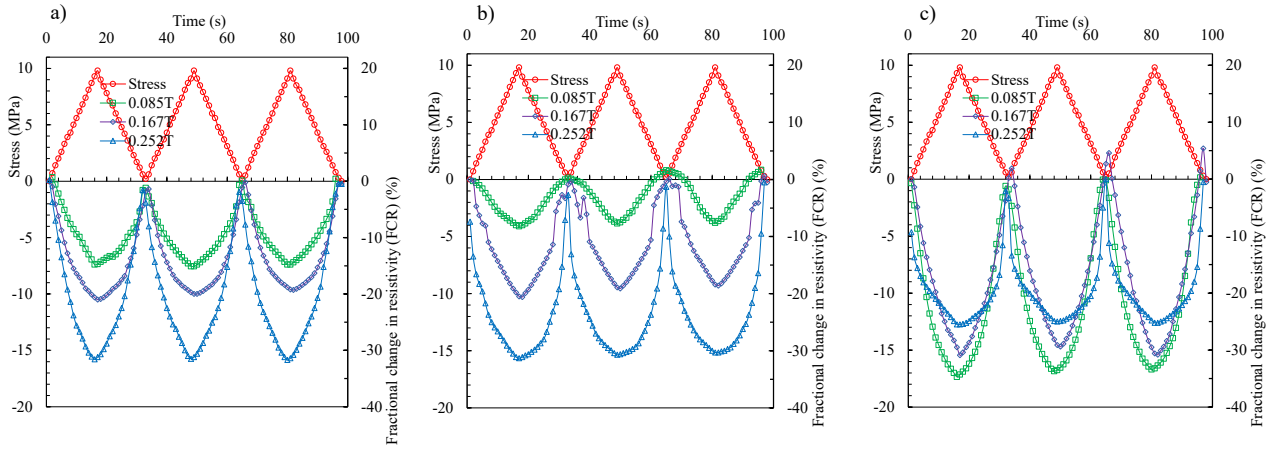

Fig. 16. The FCR of samples with a) 5 vol.%, b) 10 vol.% and c) 15 vol.% filler concentration under 0.085 T, 0.167 T and 0.252 T magnetic field flux intensity and 30 s duration.

Regarding magnetic field duration, the FCR has the same tendency as that of magnetic field strength (Fig. 17). The values are -25.1%, -18.0% and -15.9% for the samples with 5 vol.%, 10 vol.% and 15 vol.% particle contents, respectively, under 30 s magnetic field duration. It is revealed that when the duration rises to 90 s the FCR values are -7.5%, -24.9% and -26.2%, respectively. At a lower particle concentration such as 5 vol.%, it drops from -25.1% to -7.5% with increasing time duration, but exhibits a reversed trend at 10% and 15% filler content. It also emerges that under these two filler concentrations, the FCR values of the three different durations show only minimal differences, between -15% and -20%. In general, the effect of magnetic field duration on piezoresistivity is not as large as the magnetic field strength. In a lower filler concentration, the effect of different magnetic field duration is obvious, but it shows similar values when the particle content increases to 10% and 15%.

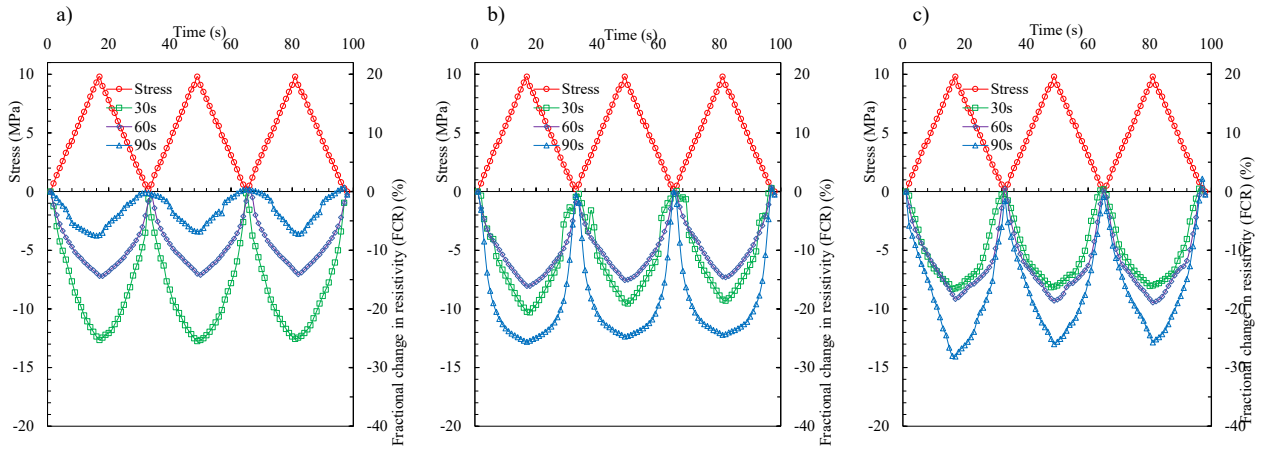

Fig. 17. The FCR of samples with a) 5%, b) 10% and c) 15% filler concentration under 30 s, 60 s and 90 s magnetic field duration and 0.167 T intensity.

4. Conclusions

This study investigated the rheological, mechanical, and electrical properties of the cement-based composite with chain-like nickel powder. The influence of the magnetic field with various strength and duration were evaluated. The microstructure was examined by SEM and X-ray CT scanning. The piezoresistive performance of the cementitious composites with oriented nickel powder fillers was significantly promoted. With these findings in mind, the major conclusions can be summarised as follows:

(1) The novel application of the magnetic field to align the nickel particles provides the cement based composites with superior electrical properties which reflected by the significant increase and drop on the electrical conductivity and the percolation threshold, respectively. Subsequently, the fractional change in resistivity and gauge factor could reach a high level due to the enhanced electron tunnelling effect. The benefit also exists in reducing the usage of nickel by taking advantage of the filler material along the direction of stress and maintaining mechanical strength and workability in the meantime.

(2) The key factor in the fabrication of the magneto-aligned sensor is the magnetic field strength and applied duration. By adjusting the magnitude of magnetic field strength, the conductive network formed by nickel powder can be optimised to achieve the best performance. The magnetic field duration, on the other hand, has less impact than the magnetic field strength.

References

1. Chen, P.-W. and D.D.L. Chung, Carbon fiber reinforced concrete for smart structures capable of non-destructive flaw detection. *Smart Materials and Structures*, 1993. **2**(1): p. 22.
2. García-Macías, E., et al., 3D mixed micromechanics-FEM modeling of piezoresistive carbon nanotube smart concrete. *Computer Methods in Applied Mechanics and Engineering*, 2018. **340**: p. 396-423.
3. García-Macías, E., et al., Micromechanics modeling of the uniaxial strain-sensing property of carbon nanotube cement-matrix composites for SHM applications. *Composite Structures*, 2017. **163**: p. 195-215.
4. Tian, Z., et al., A state-of-the-art on self-sensing concrete: Materials, fabrication and properties. *Composites Part B*, 2019. **177**.
5. Sun, M., et al., A study of piezoelectric properties of carbon fiber reinforced concrete and plain cement paste during dynamic loading. *Cement and Concrete Research*, 2000. **30**(10): p. 1593-1595.
6. Chen, P.-W. and D.D.L. Chung, Concrete reinforced with up to 0.2 vol% of short carbon fibres. *Composites*, 1993. **24**(1): p. 33-52.
7. Wen, S. and D.D.L. Chung, A comparative study of steel- and carbon-fibre cement as piezoresistive strain sensors. *Advances in Cement Research*, 2003. **15**(3): p. 119-128.
8. Chung, D.D.L., Cement reinforced with short carbon fibers: a multifunctional material. *Composites Part B: Engineering*, 2000. **31**(6): p. 511-526.
9. Gao, J., et al., Dispersion of carbon fibers in cement-based composites with different mixing methods. *Construction and Building Materials*, 2017. **134**: p. 220-227.
10. Konsta-Gdoutos, M.S. and C.A. Aza, Self sensing carbon nanotube (CNT) and nanofiber (CNF) cementitious composites for real time damage assessment in smart structures. *Cement and Concrete Composites*, 2014. **53**: p. 162-169.
11. Kim, H.K., I.S. Park, and H.K. Lee, Improved piezoresistive sensitivity and stability of CNT/cement mortar composites with low water–binder ratio. *Composite Structures*, 2014. **116**: p. 713-719.
12. García-Macías, E., et al., Micromechanics modeling of the electrical conductivity of carbon nanotube cement-matrix composites. *Composites Part B: Engineering*, 2017. **108**: p. 451-469.
13. Parvaneh, V. and S.H. Khiabani, Mechanical and piezoresistive properties of self-sensing smart concretes reinforced by carbon nanotubes. *Mechanics of Advanced Materials and Structures*, 2018: p. 1-8.
14. Li, C. and T.-W. Chou, Modeling of damage sensing in fiber composites using carbon nanotube networks. *Composites Science and Technology*, 2008. **68**(15): p. 3373-3379.
15. Chen, L., et al., Synergistic effect of conductive carbon black and silica particles for improving the pyroresistive properties of high density polyethylene composites. *Composites Part B: Engineering*, 2019. **178**: p. 107465.
16. Monteiro, A.O., P.B. Cachim, and P.M.F.J. Costa, Self-sensing piezoresistive cement composite loaded with carbon black particles. *Cement and Concrete Composites*, 2017. **81**: p. 59-65.
17. Wang, H., X. Gao, and R. Wang, The influence of rheological parameters of cement paste on the dispersion of carbon nanofibers and self-sensing performance. *Construction and Building Materials*, 2017. **134**: p. 673-683.

18. Ding, Y., et al., Effect of steel fiber and carbon black on the self-sensing ability of concrete cracks under bending. *Construction and Building Materials*, 2019. **207**: p. 630-639.
19. Ferdiansyah, T., A. Turatsinze, and J.-P. Balayssac, Design and characterization of self-sensing steel fiber reinforced concrete. *MATEC Web Conf.*, 2018. **199**: p. 11008.
20. Wen, S. and D.D.L. Chung, Self-sensing of flexural damage and strain in carbon fiber reinforced cement and effect of embedded steel reinforcing bars. *Carbon*, 2006. **44**(8): p. 1496-1502.
21. Han, B.G., et al., Development of a wireless stress/strain measurement system integrated with pressure-sensitive nickel powder-filled cement-based sensors. *Sensors and Actuators A: Physical*, 2008. **147**(2): p. 536-543.
22. Han, B., B. Han, and X. Yu, Experimental study on the contribution of the quantum tunneling effect to the improvement of the conductivity and piezoresistivity of a nickel powder-filled cement-based composite. *Smart Materials and Structures*, 2009. **18**(6): p. 065007.
23. Han, B.G., B.Z. Han, and J.P. Ou, Experimental study on use of nickel powder-filled Portland cement-based composite for fabrication of piezoresistive sensors with high sensitivity. *Sensors and Actuators, A: Physical*, 2009. **149**(1): p. 51-55.
24. Han, B., et al., Nickel particle-based self-sensing pavement for vehicle detection. *Measurement*, 2011. **44**(9): p. 1645-1650.
25. Yoo, D.-Y., I. You, and S.-J. Lee, Electrical Properties of Cement-Based Composites with Carbon Nanotubes, Graphene, and Graphite Nanofibers. *Sensors* (14248220), 2017. **17**(5): p. 1064.
26. Chen, M., et al., Mechanical and smart properties of carbon fiber and graphite conductive concrete for internal damage monitoring of structure. *Construction and Building Materials*, 2017. **142**: p. 320-327.
27. Kashif Ur Rehman, S., et al., Influence of Graphene Nanosheets on Rheology, Microstructure, Strength Development and Self-Sensing Properties of Cement Based Composites. *Sustainability* (2071-1050), 2018. **10**(3): p. 822.
28. Belli, A., et al., Evaluating the Self-Sensing Ability of Cement Mortars Manufactured with Graphene Nanoplatelets, Virgin or Recycled Carbon Fibers through Piezoresistivity Tests. *Sustainability*, 2018. **10**(11): p. 4013.
29. Dong, W., et al., Piezoresistive behaviours of carbon black cement-based sensors with layer-distributed conductive rubber fibres. *Materials & Design*, 2019. **182**: p. 108012.
30. Dong, W., et al., Electrical resistivity and mechanical properties of cementitious composites incorporating conductive rubber fibres. *Smart Materials and Structures*, 2019. **28**(8): 085013.
31. Li, H., H.-g. Xiao, and J.-p. Ou, A study on mechanical and pressure-sensitive properties of cement mortar with nanophase materials. Cement and Concrete Research, 2004. **34**(3): p. 435-438.
32. Sharma, A., et al., Nickel nanoparticles set a new record of strength. *Nature Communications*, 2018. **9**(1): p. 4102-4102.
33. Stimola, A., *Nickel*. 1st ed. Understanding the elements of the periodic table. 2007, New York: Rosen Pub. Group.
34. Beaudoin, J.J., P. Gu, and R.E. Myers, Flexural strength of cement paste composites containing micron and sub-micron nickel particulates. *Cement and Concrete Research*, 1997. **27**(1): p. 23-27.
35. Han, B., X. Yu, and J. Ou, Chapter 9 - Nickel-Powder-Based Self-Sensing Concrete, in *Self-Sensing Concrete in Smart Structures*, B. Han, X. Yu, and J. Ou, Editors. 2014, Butterworth-Heinemann. p. 271-313.
36. Han, B.G., B.Z. Han, and X. Yu, Effects of the content level and particle size of nickel powder on the piezoresistivity of cement-based composites/sensors. *Smart Materials and Structures*, 2010. **19**(6): p. 065012.
37. Han, B., X. Yu, and E. Kwon, A self-sensing carbon nanotube/cement composite for traffic monitoring. *Nanotechnology*, 2009. **20**(44): p. 445501.
38. Team, E., Smart Concrete. 2007.
39. Reza, F., J.A. Yamamuro, and G.B. Batson, Electrical resistance change in compact tension specimens of carbon fiber cement composites. *Cement and Concrete Composites*, 2004. **26**(7): p. 873-881.

40. Chung, D.D.L., A critical review of piezoresistivity and its application in electrical-resistance-based strain sensing. *Journal of Materials Science*, 2020. **55**(32): p. 15367-15396.
41. Rana, S., et al., A review on smart self-sensing composite materials for civil engineering applications. *AIMS Materials Science*, 2016. **3**(2): p. 357-379.
42. Han, B., S. Ding, and X. Yu, Intrinsic self-sensing concrete and structures: A review. *Measurement*, 2015. **59**: p. 110-128.
43. Mu, R., et al., Aligning steel fibers in cement mortar using electro-magnetic field. *Construction and Building Materials*, 2017. **131**: p. 309-316.
44. Xiao, H., M. Liu, and G. Wang, Anisotropic electrical and abrasion-sensing properties of cement-based composites containing aligned nickel powder. *Cement and Concrete Composites*, 2018. **87**: p. 130-136.
45. Chen, B., K. Wu, and W. Yao, Conductivity of carbon fiber reinforced cement-based composites. *Cement and Concrete Composites*, 2004. **26**(4): p. 291-297.
46. Wen, S. and D.D.L. Chung, The role of electronic and ionic conduction in the electrical conductivity of carbon fiber reinforced cement. *Carbon*, 2006c. **44**(11): p. 2130-2138.
47. Chen, P.-W. and D.D.L. Chung, Carbon-Fiber-Reinforced Concrete as an Intrinsically Smart Concrete for Damage Assessment during Dynamic Loading. *Journal of the American Ceramic Society*, 1995b. **78**(3): p. 816-818.
48. D'Alessandro, A., et al., Investigations on scalable fabrication procedures for self-sensing carbon nanotube cement-matrix composites for SHM applications. *Cement and Concrete Composites*, 2016. **65**: p. 200-213.
49. Sun, S., et al., Nano graphite platelets-enabled piezoresistive cementitious composites for structural health monitoring. *Construction and Building Materials*, 2017. **136**: p. 314-328.
50. Wen, S. and D.D.L. Chung, Piezoresistivity-Based Strain Sensing in Carbon Fiber-Reinforced Cement. *ACI Materials Journal*, 2007. **104**(2): p. 171-179.
51. Ou, J. and B. Han, Piezoresistive Cement-based Strain Sensors and Self-sensing Concrete Components. *Journal of Intelligent Material Systems and Structures*, 2009. **20**(3): p. 329-336.
52. Azhari, F. and N. Banthia, Cement-based sensors with carbon fibers and carbon nanotubes for piezoresistive sensing. *Cement and Concrete Composites*, 2012. **34**(7): p. 866-873.
53. Vilaplana, J.L., et al., Self-Sensing Properties of Alkali Activated Blast Furnace Slag (BFS) Composites Reinforced with Carbon Fibers. *Materials* (Basel, Switzerland), 2013. **6**(10): p. 4776-4786.
54. Li, X. and M. Li, Multifunctional self-sensing and ductile cementitious materials. *Cement and Concrete Research*, 2019. **123**: p. 105714.
55. Al-Dahawi, A., et al., Effect of mixing methods on the electrical properties of cementitious composites incorporating different carbon-based materials. *Construction and Building Materials*, 2016. **104**: p. 160-168.
56. Al-Dahawi, A., et al., Electrical percolation threshold of cementitious composites possessing self-sensing functionality incorporating different carbon-based materials. *Smart Materials and Structures*, 2016. **25**(10): p. 105005.
57. Yıldırım, G., et al., Self-sensing capability of Engineered Cementitious Composites: Effects of aging and loading conditions. *Construction and building materials*, 2020. **231**: p. 117132.
58. Tian, Z., et al., Influence of particle morphology and concentration on the piezoresistivity of cement-based sensors with magneto-aligned nickel fillers. *Measurement*, 2021. In press.